Journal of Power Sources 216 (2012) 417–424

Contents lists available at SciVerse ScienceDirect

Journal of Power Sources

journal homepage: www.elsevier.com/locate/jpowsour

Performance and short-term stability of single-chamber solid oxide fuel cells based on $La_{0.9}Sr_{0.1}Ga_{0.8}Mg_{0.2}O_3-\delta$ electrolyte

M. Morales [a,*], J.J. Roa [b], J. Tartaj [c], M. Segarra [a]

[a] DIOPMA Centre, Departament de Ciència dels Materials i Enginyeria Metal·lúrgica, Facultat de Química, Universitat de Barcelona, Martí i Franquès 1, 08028 Barcelona, Spain
[b] Institute Pprime, Laboratoire de Physique et Mécanique des Matériaux, CNRS-Université de Poitiers-ENSMA, UPR 3346, Bd Pierre et Marie Curie, BP 30179, 86962 Futuroscope Chasseneuil Cedex, France
[c] Instituto de Cerámica y Vidrio (CSIC), Kelsen 5, 28049 Cantoblanco, Madrid, Spain

HIGHLIGHTS

- Electrical properties of cells with LSGM electrolyte operated in methane–air mixtures.
- Cell performance was not significantly affected operating under optimal SC-SOFC conditions.
- Operating conditions to minimize the degradation of electrodes at short-term were well established.
- Performance stability of buffered cell at short-time was similar to that for non-buffered one.

ARTICLE INFO

Article history:
Received 17 January 2012
Received in revised form
10 May 2012
Accepted 16 May 2012
Available online 1 June 2012

Keywords:
Solid oxide fuel cells
Lanthanum gallate
Single-chamber fuel cell
Methane
Buffer layer

ABSTRACT

In the present work, the performance of $La_{0.9}Sr_{0.1}Ga_{0.8}Mg_{0.2}O_3$ (LSGM) electrolyte-supported SOFCs was evaluated under single-chamber conditions. For this purpose, two single cells, one with and the other without $Sm_{0.2}Ce_{0.8}O_{3-\delta}$ (SDC) buffer layer between anode and electrolyte, were studied in order to determine and compare the performance and short-term stability of cells under single-chamber conditions. The reactivity of the Ni-SDC anode with SDC (for the cell with buffer layer) and the LSGM electrolyte (for the cell without buffer layer) were studied by X-ray diffraction. The reaction between Ni and LSGM during anode sintering and cell operation leads to a substantial loss in the cell performance when no buffer layer is present. As a result, maximum power densities of 246 and 132 mW cm^{-2} were obtained for the buffered and non-buffered cells respectively, at 800 °C, under optimized gas composition ($CH_4/O_2 = 1.2$) and a total flow rate of 400 ml min^{-1}. After 55 h operating at 750 °C and 6 thermal cycles, the performances of both cells were decreased around 25–30 mW cm^{-2}.

1. Introduction

Single-chamber solid oxide fuel cells (SC-SOFCs), in which both anode and cathode are exposed to the same mixture of fuel and oxidant gas, have been intensively investigated for the last decade [1]. The main advantage of SC-SOFCs, with respect to traditional dual-chamber SOFCs, is to simplify the device design and to operate in mixtures of hydrocarbon (methane, propane…) and air, without separation between fuel and oxidant [2,3], which is known as internal reforming, as their operating temperatures are optimal for hydrocarbon reforming in the anode [4,5]. SOFCs under these conditions become thermally and mechanically more resistant than conventional fuel cells. Owing to the exothermic nature of the fuel oxidation reactions, the cell temperature is much higher than the furnace temperature, thus enhancing the ion conductivity of the electrolyte and the catalytic activity of the electrodes. It allows self-sustained SC-SOFC to be possible [6]. Another advantage of this cell operation type is that the poisoning of the Ni by deposition of carbon or sulphur cannot be possible, as the presence of oxygen at the electrode oxidizes both elements.

Initially, the research in the SC-SOFCs and the dual-chamber SOFCs was focused on the $Y_{0.08}Zr_{0.92}O_{1.96}$ (YSZ) electrolyte cells [1–6]. However, it requires high operating temperatures (800–1000 °C) to obtain high ionic conductivity, thus resulting in several problems for the cells: undesirable chemical reactions between cell components, ageing of components, and thermal expansion mismatch [1], thus accelerating the decrease of the cell performance. In order to decrease the operating temperature to 600–800 °C, it is necessary to reduce the electrolyte specific resistance, so electrolytes with higher ionic conductivities than YSZ at low and intermediate operating temperatures must be used. A

* Corresponding author. Tel.: +34 93421316; fax: +34 934035438.
E-mail addresses: mmorales@ub.edu, mmoralescomas@yahoo.es (M. Morales).

0378-7753/$ – see front matter © 2012 Elsevier B.V. All rights reserved.
doi:10.1016/j.jpowsour.2012.05.076

common strategy is the replacement of YSZ electrolyte by doped ceria materials [7,8]. However, Ce^{4+} of ceria-based electrolytes is partly reduced to Ce^{3+} at intermediate temperatures and low oxygen partial pressures, which results in some electronic conductivity [7,9]. So, the electronic conductivity in the electrolyte can lead to a reduction of the open-circuit voltage (OCV) and power density.

In contrast, the Sr and Mg doped $LaGaO_3$ materials ($La_{1-x}Sr_xGa_{1-y}Mg_yO_{3-\delta}$, LSGM) present high oxygen-ion conductivities at intermediate temperatures (>0.1 S cm^{-1} at 800 °C) [10,11], and a wide range of oxygen partial pressures ($10^{-21} < P(O_2) < 0.1$) [12,13]. Several works have demonstrated good cell performances using LSGM as electrolyte. Dokyol Lee et al. [14] obtained a performance of 664 mW cm^{-2} at 800 °C, using $La_{0.8}Sr_{0.2}Ga_{0.8}Mg_{0.2}O_{2.8}$, which exhibited the highest electrical conductivity among LSGMs of various compositions. Wan et al. [15] prepared a single SOFC with a $La_{0.8}Sr_{0.2}Ga_{0.83}Mg_{0.17}O_{2.815}$ electrolyte 200 μm thick and a $La_{0.4}Ce_{0.6}O_{1.8}$ buffer layer 20 μm thick between the electrolyte and the two electrodes, which achieved a power density as high as 1.4 W cm^{-2} at 800 °C. Despite these advantages, LSGM is not widely used as electrolyte for SOFCs, as it may present important chemical reactions with electrodes. The interfacial reaction between Ni-based anode and LSGM electrolyte, during the sintering process at high temperature, has been reported in several works [16,17]. It induces the formation of resistive phases, such as $LaSrGa_3O_7$, $LaSrGaO_4$ or $LaGaO_4$, at the interface anode–electrolyte, thus causing a strong drop in the cell performance [18,19]. A potential solution to avoid the interfacial reactions is to decrease the co-sintering temperature of the anode–electrolyte at ones lower than 1300 °C, which is difficult to perform according to the typical manufacturing process of LSGM anode-supported SOFCs [16]. Another choice is to use a buffer layer, based on doped ceria, between the anode and the electrolyte, which can suppress Ni and La migration [17,20]. Alternatively, the combination of LSGM electrolyte-supported design and the anode–electrolyte buffer layer of doped ceria may minimize the interfacial reactions, as the anode sintering temperature for this configuration is lower than that for anode–electrolyte co-sintering one of an anode-supported cell [15,17].

Owing to the chemical reactions between the LSGM electrolyte and the electrodes, few studies about LSGM cells have been reported and much less literature is available about the SC-SOFCs using this electrolyte [2,6]. In the present work, $La_{0.9}Sr_{0.1}Ga_{0.8}Mg_{0.2}O_3-\delta$ electrolyte-supported SOFCs were evaluated under single-chamber conditions, using a mixture of methane and synthetic air. For this purpose, both single cells with and without $Sm_{0.2}Ce_{0.8}O_{3-\delta}$ (SDC) buffer layer between anode and electrolyte were studied in order to determine and compare the performance and short-term stability of cells under single-chamber conditions.

2. Experimental

2.1. Fuel cell preparation

Electrolyte and electrode powders for single-chamber fuel cells were prepared by sol–gel related methods. $La_{0.9}Sr_{0.1}Ga_{0.8}Mg_{0.2}O_{3-\delta}$ electrolyte powders were prepared by the polymeric organic complex solution method. Aqueous solutions of corresponding nitrates were mixed by stirring with nitric acid (65%) and ethylene glycol (1:8 vol:vol) to make a gel. The ash-obtained solutions were thermally treated in three steps: 80 °C for 2 h, 120 °C for 3 h, to obtain a black resin embedding all the cations, and finally 180 °C up to the combustion of the polymeric gel. After milling in an agate mortar, the resin was calcined at 1000 °C for 5 h, and attrition milled for 2 h in ethanol with zirconia balls. $La_{0.5}Sr_{0.5}CoO_{3-\delta}$ (LSC) cathode powders were prepared by the citrate sol–gel method starting from nitrate solutions of the different elements [21].

Cylindrical pellets of LSGM electrolytes were prepared from LSGM powders by uniaxial pressing at 200 MPa. A SDC buffer layer was deposited via screen printing on a side of a pellet. According to previous works [13,14], both pellets with and without a buffer layer were then sintered in air at 1400 °C for 5 h. Final disks presented a diameter of 12 mm and a thickness of 200 μm. For anode preparation, an ink was prepared from a powder mixture of Ni–SDC (70–30 wt.%) and a commercial resin. For this purpose, a commercial Ni (ALDRICH, 99.9% purity and 2.2–3 μm average particle size) was used. The ink was deposited by screen printing on the side of the SDC buffer layer and directly on the LSGM pellet without buffer layer. According to previous studies [16,17,22,23], an anode sintering temperature within range of 1100–1300 °C for 2–6 h, using a thickness of doped-ceria buffer layer between 10 and 20 μm, and a cathode as it will be presented later, may be suitable to prevent the anode–electrolyte interfacial reactions and obtain a good cell performance. Our preliminary experiments, which were based on electrical measurements of cell performance and ohmic resistance, revealed that anode sintered in a 5% H_2–Ar flow (50 ml min^{-1}) at 1100 °C for 2 h, using a SDC buffer layer 10 μm thick, was appropriated to achieve the highest cell performance. When the anode sintering temperature was equal or higher than 1200 °C, even for a buffer layer thickness around 20 μm, the performance of cell was lower than that of optimal sintering conditions. Only if the temperature of anode formation was not lower than 1100 °C, electrical properties of cell and adherence between anode and SDC (or LSGM for cell without buffer layer) were satisfactory.

For cathode preparation, a powder mixture of LSC–SDC–Ag_2O (80–10–10 wt.%) was prepared. The LSC and SDC powders were homogenized with 10 wt.% Ag_2O in an agate mortar, and mixed with the same commercial resin. Then, the ink was deposited by screen printing directly on the other side of the dense LSGM electrolytes. As a previous work [24], cathode was sintered in an argon flow (50 ml min^{-1}) at 1000 °C for 2 h. Finally, fuel cells presented a final diameter of 12 mm, with an electrolyte thickness of 200 μm and an anode and cathode thickness of 20–30 μm each one. The active area of the fuel cell was around 50 mm^2. The microstructures of the fuel cells were observed using a JEOL JSM-840 scanning electron microscope (SEM). After that, the presence of the interfacial reactions at the different interfaces of both cells was analysed by energy dispersive X-ray analysis (EDX) in the deep range of 1–10 μm. Finally, the reactivity of the anode, buffer layer and cathode with LSGM was studied in order to analyse the chemical compatibility of the materials, thus identifying the secondary phases formed during the manufacturing process. Chemical reactivity experiments were performed with the mixture powders of NiO, SDC, and LSC with LSGM (1:1 wt. ratio), respectively.

2.2. Electrical characterization of the cells under single-chamber conditions

In order to determine the electrical properties, platinum wires were attached to the electrode surfaces of the fuel cells for current collection. An ink of LSC–SDC–Ag_2O (80–10–10 wt.%) was deposited on the cathode as current collector. For the current contact in the anode, an ink of Ni–SDC (90–10 wt.%) and the same commercial resin were used. In addition, Ag mesh was used as an electronic collector for cathode. Moreover, an additional thermocouple Pt versus Pt–10% Rh was placed in direct contact with the centre of the anode surface in order to determine the real temperature of the fuel cells. The cells were placed in a quartz tube (inner diameter 23 mm), where a mixture of $N_2 + O_2$ with the air

composition (80:20%, respectively) was flown with different methane mixtures between 0.8 and 1.6 of CH_4/O_2 ratio, and total flux rates from 200 up to 700 m min^{-1}. Then, the fuel cells were heated inside the quartz tube by a tubular furnace at 5 °C min^{-1}, from room temperature to 850 °C. Electromotive forces (emfs) were measured using a Keithley 617 electrometer with an input resistance of 1014 Ω. The value of current was measured by recording the voltage drop in an auxiliary known resistance. The characteristic intensity to voltage curves (I–V) were determined by using the equipment for measuring current and voltage under variable loads.

2.3. Efficiency and stability of the SC-SOFCs

In analogy to our previous studies [19], the cell performance stability, fuel utilization factor, and efficiency were investigated under different operating conditions. The electrochemical fuel utilization factor (U_f) represents the ratio of fuel amount consumed in the SOFC to the amount of supplied fuel. However, U_f inside a SOFC can be also calculated by the cell current, I, and the inlet fuel (methane) [25]:

$$U_f = \frac{I}{F \cdot [6 \cdot n(CH_4\text{inlet})]} \quad (1)$$

where F is Faraday's constant and $n(CH_4)$ is the inlet number of methane moles. For a single-chamber SOFC, the most representative parameter is to determine the U_f, because the methane reacts with O_2 to produce H_2 and CO (reforming reaction) and these products can be utilized as fuel to generate electrical current (electrochemical reaction). Another important parameter is the system efficiency (η), which is normally calculated as the useful power generated by a specific cell with respect to the fuel input, specifying the low or high heat values for the fuel:

$$\eta = \frac{\text{system power output}}{\text{lower heating value of fuel}} = \frac{P_{max}}{\Delta H_{reaction}} \quad (2)$$

where P_{max} is the corresponding power drawn from the cell, and $\Delta H_{reaction}$ represents the enthalpy of reaction for the overall reaction corresponding to total oxygen consumption from the mixture at the undergoing CH_4/O_2 ratio value. In this way, the gas mixture is passing only once through the cell compartment, without fuel recycling. For a single-chamber SOFC, the best efficiency occurs at the maximum specific power. It is due to that the cell power output does not significantly depend on the methane consumed by reforming reaction, and the generated heat by system reactions (reforming reaction and electrochemical reactions) is not used for some type of cogeneration [4,26].

On-line gas chromatography (Agilent Micro GC 3000) was used to analyse the effluent gases. Calculations of the different species were based on the fact that N_2 (carrier gas) was not consumed or formed during the experiment, and the total number of moles of this specie remained constant during the entire test. So, N_2 was used as an internal standard. Reactant consumptions of CH_4 and O_2, and product concentrations of H_2, CO and CO_2 were calculated as follows:

$$\text{Consumption of } R(\%) = \frac{\text{moles of}[R(\text{in}) - R(\text{out})]}{\text{moles of } R(\text{in})} \cdot 100 \quad (3)$$

$$\text{Conc. of } P(\%) = \frac{\text{moles of } P(\text{out})}{\text{moles of}[(N_2 + CH_4 + O_2 + H_2 + CO + CO_2)(\text{out})]} \cdot 100 \quad (4)$$

where $R = CH_4$ or O_2, and $P = H_2$, CO or CO_2. Before testing the cells, several blanks were performed to confirm the absence of direct oxidation reactions in the furnace atmosphere. Blank tests were carried out under similar conditions to the electrical tests of the fuel cells.

Finally, the stability of both cells as a function of the time and thermal cycles under different operating conditions was analysed. This study was divided in two parts, because the performance stability in the SC-SOFCs critically depends on the electrodes degradation. First of all, the stability of each electrode was studied to determine the effect of the operating conditions on the degradation of electrodes. Afterwards, the global stability of both cells as a function of the time and thermal cycles was analysed under optimized operating conditions, thus minimizing the degradation of electrodes. In order to evaluate the performance of LSGM cells at short-time and several thermal cycles, a test of 55 h with 6 thermal cycles was performed on each cell at 750 °C.

3. Results and discussion

3.1. Microstructural characterization

Fig. 1 shows the SEM micrographs of the Ni–SDC/SDC/LSGM/LSC–SDC–Ag_2O and Ni–SDC/LSGM/LSC–SDC–Ag_2O microstructures for both cells after manufacturing process. For both cells, the electrolytes presented high density, and the anode–electrolyte and electrolyte–cathode interfaces exhibited a good interfacial adhesion. Moreover, it was also observed that the SDC buffer layer, which had a thickness around 10 μm, was well adhered to both LSGM electrolyte and Ni–SDC anode. The porosity of electrodes is not clearly observed in the images of buffered cell, due to that the cell cross-section was polished, thus partially closing the pores, to view the buffer layer by SEM.

3.2. Chemical compatibility of materials

Fig. 2 shows the results of the energy dispersive X-ray analysis (EDX) in order to determine if any chemical reaction and/or diffusion was produced at the interfaces between the anode and the electrolyte of both cells in the deep range of 1–10 μm. Small amounts of Ni phase were detected at the LSGM electrolyte of the cell without a buffer layer (Fig. 2a). The presence of small amounts of La in the anode was also observed. In contrast, the buffer layer of another cell blocked the La and Ni migration between the anode and the electrolyte (Fig. 2b). Both anode and electrolyte did not exhibit contamination by species based on SDC layer. However, small amounts of Ni and La were detected into the SDC layer, which were diffused from anode and electrolyte to buffer layer, respectively. So, a small loss of La with respect to the original LSGM composition was observed, thus resulting in La-deficient phases at the LSGM side. On the other hand, electrolyte–cathode interface was also analysed. Low intensity peaks of Ga and Co were detected in punctual zones of the cathode and electrolyte, respectively, which were in a good agreement with the results presented by others authors [27].

Afterwards, the chemical compatibility of the NiO, SDC, and LSC with LSGM was studied by X-ray diffraction. Fig. 3 a–b shows the X-ray diffraction patterns of LSGM and a mixture powders of NiO–LSGM (1:1 wt. ratio) after firing at 1100 °C for 2 h. It clearly indicated the formation of typical non-conductive phases: $LaSrGa_3O_7$ and $LaSrGaO_4$. The formation of the La-deficient phase at the LSGM side was closely related to the migration of La from LSGM electrolyte to the ceria-based buffer layer. The $LaNiO_3$ phase was also formed, as some peaks of both $LaNiO_3$ and LSGM phases appear overlapped, thus causing that these signs of NiO–LSGM were wider than those of pure LSGM phase (Fig. 3a). Probably, these resistive phases were formed at the interface anode–electrolyte of the cell without buffer layer. Zhang et al. [16] reported that $LaNiO_3$ was

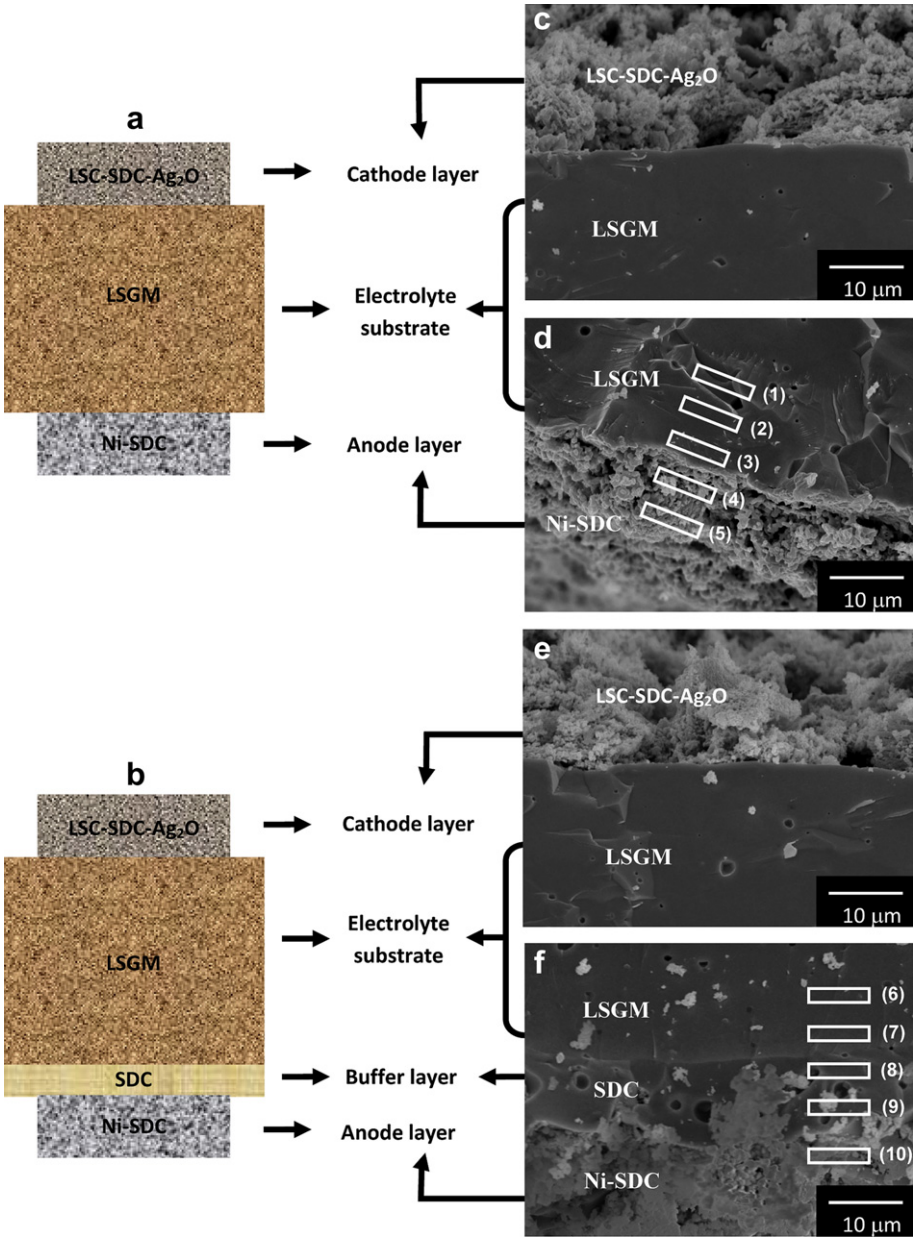

Fig. 1. Schematic configurations of the LSGM electrolyte-supported cells: (a) without and (b) with SDC buffer layer. SEM micrographs of the cross-sectional of the post-mortem SOFCs: (c) cathode–electrolyte, (d) electrolyte–anode of the cell without SDC buffer layer; and (e) cathode–electrolyte, (f) electrolyte–buffer-layer–anode of the cell with a SDC buffer layer. Numbers indicate the areas where EDX analyses were performed (see Fig. 2).

detected from X-ray diffraction patterns of an LSGM–NiO mixture at 1:1 weight ratio after sintering at 1150 °C for 2 h. Our results confirmed that NiO and LSGM are chemically incompatible materials under the anode sintering conditions of 1100 °C for 2 h. On the other hand, Fig. 3c shows the powder X-ray diffraction patterns of the SDC–LSGM (1:1 wt. ratio) mixture after firing at 1400 °C for 5 h. Several new peaks appeared after firing, which corresponds to the $LaSrGa_3O_7$ and $LaSrGaO_4$, which was attributed to the diffusion of La from LSGM to SDC to form $Ce_{1-x}La_xO_{2-2x/2}$ [14,28]. It is due to that the rare earth ions, such as La, Sm, or Gd, have a good solubility in the CeO_2 fluorite phase, because of their close ionic radius and structure of their oxides [29]. Despite SDC layer was originally introduced to suppress chemical reaction between the anode and electrolyte, it is clear that there are diffusion reactions between the LSGM and the SDC under the test conditions. However, the ceria buffer layer could block the Ni migration across the LSGM/NiO–GDC interface, thus avoiding the formation of the Ni rich phase ($LaNiO_3$) at the LSGM side. Finally, the X-ray diffraction patterns of the LSC–LSGM (1:1 wt. ratio) mixture, sintered at 1000 °C for 2 h, showed two perovskite phases: LSC and LSGM (Fig. 3d). The mixture LSC/LSGM apparently presented no remarkable signs of reaction in sintering powders, thus indicating that LSC is a chemically compatible cathode material with LSGM electrolyte, under the cathode sintering conditions of 1000 °C for 2 h. These results are in good agreement with the EDX analysis of the electrolyte–cathode interface presented in Fig. 2, which revealed a slight diffusion between cathode and electrolyte. It can be attributed to the relatively low sintering temperature of cathode. Similar results were obtained by other authors using the same materials and sintering temperatures [27].

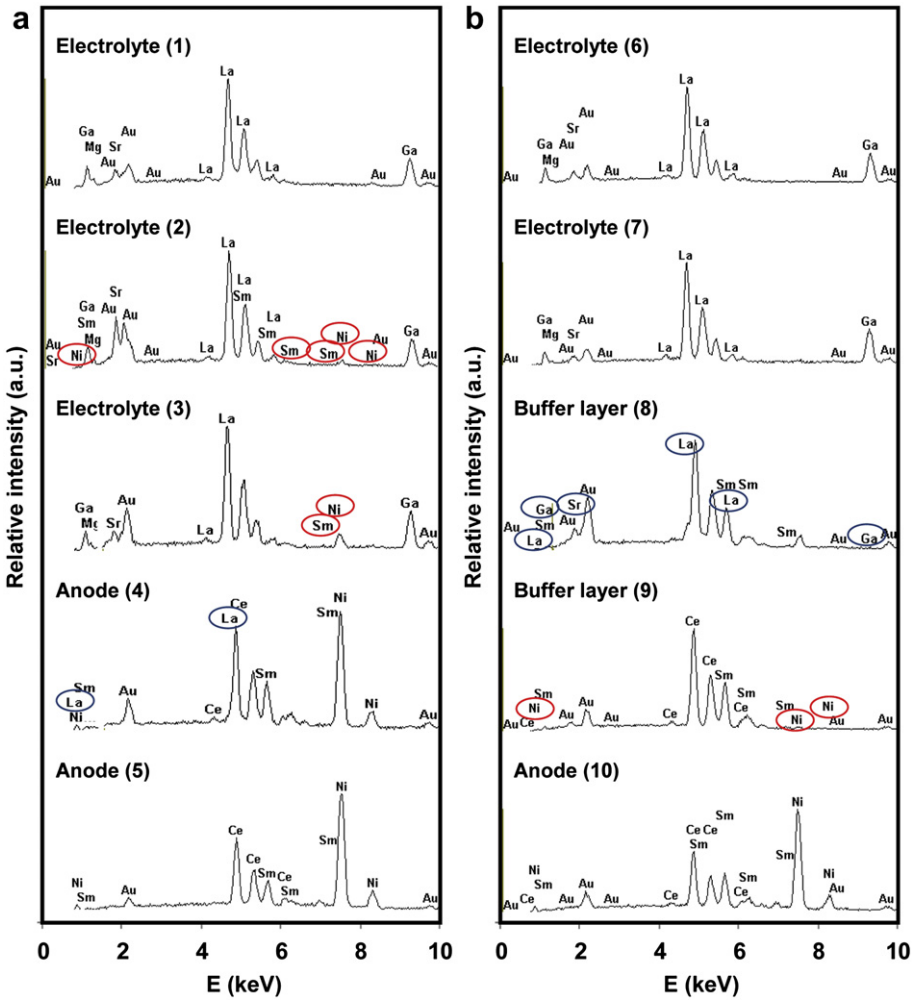

Fig. 2. EDX analysis of: (a) NiO–SDC/LSGM and (b) NiO–SDC/SDC/LSGM interfaces corresponding to non-buffered and buffered cells, respectively. Numbers indicate the location of each analysis in Fig. 1.

3.3. Cell performance of the single cells

Electrical characterization of both cells in open circuit voltage (OCV) is an important parameter in SC-SOFCs, because it gives an idea of the heterogeneous catalysis of the hydrocarbon and the oxygen species at the anode. It also indicates the selectivity of the cathode for the oxygen electro-reduction. Moreover, they can strongly differ as a function of different operating parameters such as the gas composition and the total flow rate [19,30]. Preliminary experiments revealed that the highest OCV of the cells was obtained at a CH_4/O_2 ratio between 1.2 and 1.7. The influence of total flow rate (methane + air) on the OCV was also studied, thus obtaining that the OCV remains almost constant between 400 and 700 ml min^{-1}. So, subsequent experiments for both cells were performed at a CH_4/O_2 ratio of 1.2 and a total flow rate of 400 ml min^{-1}. Then, the influence of temperature on the OCV was evaluated under optimizing conditions of gas composition and total flow rate. High reproducibility of cell performances was observed in both systems after testing three identical cells for each cell type for several hours.

As shown in Fig. 4, the OCV slightly decreases with increasing temperature within range of 690–800 °C. It is noted that OCVs of the cell with a SDC buffer layer were slightly higher than those of the cell without a buffer layer. Values of 0.97 and 0.92 V at 680 °C with and without a SDC buffer layer were achieved respectively. According to the results in Fig. 4, the interfacial reactions between Ni-based anode and LSGM electrolyte, which took place during the sintering processes and operating time, slightly decreased the OCVs of the non-buffered cell. The formation of the undesired $LaNiO_3$ phase at the anode–electrolyte interface of the non-buffered cell could cause the loss of voltage with respect to cell OCV with buffer layer. Probably, the H_2 and CO generation at anode–electrolyte interface, which depends on the catalytic activity of the methane reforming, was slightly reduced by the presence of small amounts of $LaNiO_3$. Thus, the highest OCVs achieved for both cells were comparable to the values obtained by other researchers, which obtained between 0.9 and 1.0 V under similar operating conditions of SC-SOFCs, and using an electrolyte based on doped $LaGaO_3$, Ni cermet as an anode, and Co-based perovskites as a cathode [2,6].

On the other hand, Fig. 5 shows *I–V* (current density and cell voltage) and *I–P* curves (power density derived from *I–V*) for both fuel cells. Performances of 164 mW cm^{-2} at 700 °C and 246 mW cm^{-2} at 800 °C were achieved for the buffered cell, whereas the power densities for the non-buffered cell were 92 mW cm^{-2} at 700 °C and 132 mW cm^{-2} at 800 °C. So, both power and current densities of the cell with a buffer layer were higher than those of the one without a buffer layer. It was attributed to the formation of resistive secondary phases, which strongly increased the internal ohmic resistance in the non-buffered cell [17]. The migration of La and Ga from LSGM electrolyte generated the

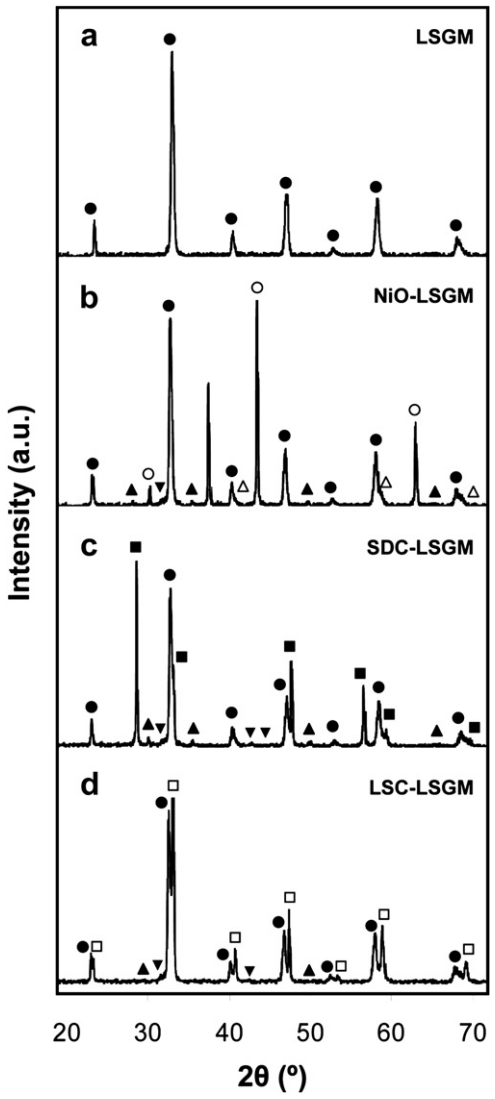

Fig. 3. X-ray diffraction patterns of: (a) LSGM after firing at 1400 °C for 5 h; (b) LSGM–NiO (1:1 wt. ratio) 1100 °C for 2 h; (c) LSGM–SDC (1:1 wt. ratio) 1400 °C for 5 h; and (d) LSGM–LSC (1:1 wt. ratio) 1000 °C 2 h. Symbols of phases: $La_{0.9}Sr_{0.1}Ga_{0.8}Mg_{0.2}O_{3-\delta}$ (●), $LaSrGa_3O_7$ (▲), $LaSrGaO_4$ (▼), $LaNiO_3$ (△), NiO (○), $Sm_{0.2}Ce_{0.8}O_{3-\delta}$ (■), and $La_{0.5}Sr_{0.5}CoO_{3-\delta}$ (□).

formation of La deficient LSGM phases, such as $LaSrGa_3O_7$ and $LaSrGaO_4$, at the anode–electrolyte interface. These secondary phases produced an ohmic resistivity higher than that of $La_{0.9}Sr_{0.1}Ga_{0.8}Mg_{0.2}O_{3-\delta}$ phase, which increased the cell resistance at the anode–electrolyte interface, thus decreasing the power density of the cell. Furthermore, the formation of the $LaNiO_3$ perovskite was also possible, which is a poor oxide-ion conductor, thus contributing to the increase of the resistance at the anode–electrolyte interface. The performances obtained in the present work were comparable to those of Hibino et al. [2,6], which reported maximum power densities around 350 and 450 mW cm^{-2} for an electrolyte-supported SC-SOFC using $La_{0.9}Sr_{0.1}Ga_{0.8}Mg_{0.2}O_{3-\delta}$ as an electrolyte (0.18 mm thickness) and methane as fuel at 700 and 800 °C, respectively. On the other hand, Fukui et al. [31] reported power densities over 0.7 W cm^{-2} at 800 °C and 0.4 W cm^{-2} at 700 °C in a cell with a $La_{0.9}Sr_{0.1}Ga_{0.8}Mg_{0.2}O_{3-\delta}$ electrolyte of 130 μm of thickness prepared by tape casting, LSC as a cathode, and NiO–$(CeO_2)_{0.8}(SmO_{0.15})_{0.2}$ (NiO–SDC) as an anode material, operating with 97% H_2 + 3% H_2O as fuel and air as oxidant.

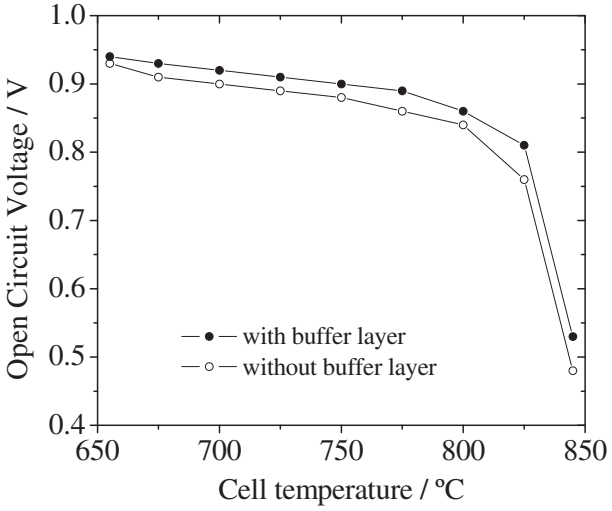

Fig. 4. Open circuit voltage (OCVs) as a function of the temperature for both SC-SOFCs, with and without using a SDC buffer layer, at a CH_4/O_2 ratio of 1.2 and a total flow rate of 400 ml min^{-1}.

Our power densities were significantly lower than Fukui's values, due to that they operated in dual-chamber with a fuel highly concentrated in H_2. In comparison with our previous work [29], the OCVs and voltages at low current densities of cells based on LSGM electrolyte are higher than those of doped ceria SOFCs, thus obtaining higher performance and efficiency. Therefore, the use of LSGM as electrolyte may be advantageous whether interfacial reactions are minimized.

3.4. Efficiency of the single cells

A fuel utilization factor of 14% was obtained for the cell with buffer layer under optimized conditions: a CH_4/O_2 ratio of 1.2, a total flow rate of 400 ml min^{-1}, a temperature of 750 °C (210 mW cm^{-2} of power density) and an electrode area of 0.5 cm^2. The electrochemical fuel utilization factor for the same cell and operating conditions was 1.3%. On the other hand, the cell efficiency, calculated under optimal operating conditions and $\Delta H_{react} \sim -300$ kJ/mol, was 0.8%. These values are higher than those published in our previous work [21], which were obtained for

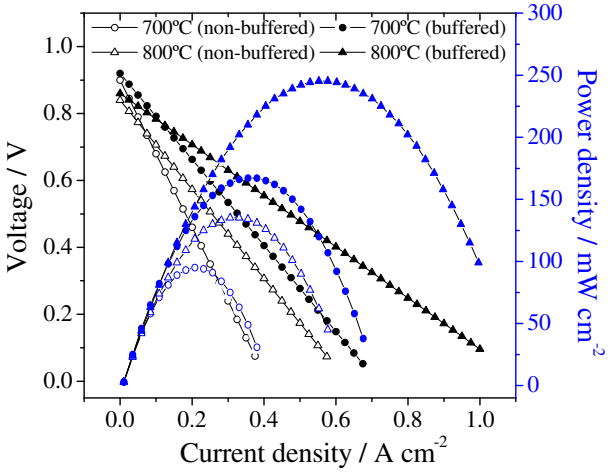

Fig. 5. Voltage and power density vs. current density for both cells, operating at different cell temperatures, a CH_4/O_2 ratio of 1.2 and a total flow rate of 400 ml min^{-1}.

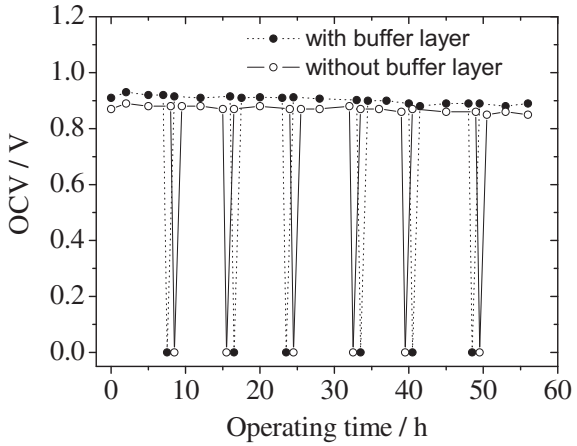

Fig. 6. Open circuit voltage (OCVs) as a function of the operating time and thermal cycles for both fuel cells, operating at a cell temperature of 750 °C, a CH_4/O_2 ratio of 1.2, and a total flow rate of 400 ml min^{-1}.

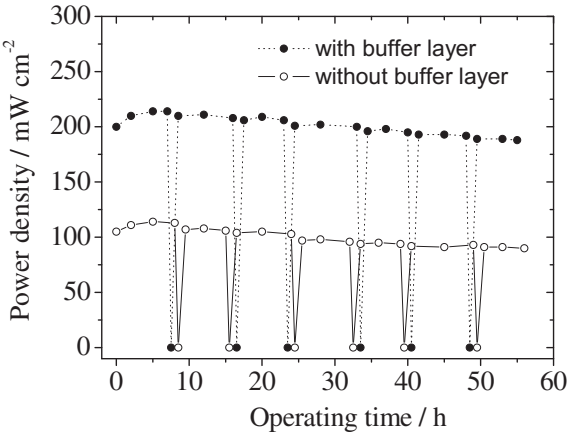

Fig. 7. Power density as a function of the operating time and thermal cycles for both fuel cells, operating at a cell temperature of 750 °C, a CH_4/O_2 ratio of 1.2 and a total flow rate of 400 ml min^{-1}.

an anode-supported cell with GDC as electrolyte and also operated under SC-SOFC configuration. Since the performance in both cells is similar, the difference in efficiency for both cells is partially due to that the methane consumption of the electrolyte-supported cell is less than that of an anode-supported one. In this second cell design, both thickness and anode area, which are directly related to the cell reforming, were larger than for the electrolyte-supported cell. Another reason is that the anode-supported cell was exposed, under optimal operating conditions, at a higher total flow rate (530 ml min^{-1}) than that used in the present work (400 ml min^{-1}). On the other hand, these efficiency values are similar to those of Napporn et al. [4] ($U_f = 3.6\%$) and Shao et al. [32] ($\eta \sim 1\%$) using methane and propane as fuels in anode-supported SC-SOFCs. In comparison to double-chamber cells, the efficiencies for the single-chamber SOFCs are quite lower [20]. Furthermore, it should also take into account that the reactor design was not optimized to enhance the cell efficiency. The chamber diameter dimension of the reactor was much larger than that of cell, thus resulting in a significant amount of methane exiting the reactor without being consumed.

3.5. Short-term stability of electrodes and cells

Preliminary works revealed that the stability of the cell performance significantly decreased when increasing the number of thermal cycles, due to that both anode and cathode were degraded by the redox cycles. In order to minimize the degradation process, the solution was to maintain the cell under inert gas (N_2), when the temperature was below 650 °C, thus avoiding the anode oxidation. Moreover, it was necessary to work at cell temperatures below 780 °C, because the LSC was partially reduced at higher temperatures. For this reason, the stability of LSC was analysed by X-ray diffraction under different operating conditions. When the cathode generated only CO_2 and H_2O, and low concentrations of H_2 and CO (below 780 °C), LSC presented the initial cubic structure. In contrast, the partial decomposition of a LSC fraction was observed at 825 °C for 15 min, due to that the cathode produced high concentrations of H_2 and CO. Then, La_2O_3, SrO, CoO, and Co phases appeared, and the intensities of the diffraction peaks attributed to $La_{0.5}Sr_{0.5}CoO_{3-\delta}$ significantly decreased. Therefore, the cell performance decreased by the extreme operating conditions in temperature (>790 °C) and time (>5 min). However, the performance was not affected, when the cell was punctually operated (for 5 min) in these extreme conditions, or when it worked under optimized conditions ($680 < T < 750$ °C and $1.2 < CH_4/O_2 < 1.7$). According to these results, the operating conditions to avoid the electrode degradation were well established.

A test of 55 h with 6 thermal cycles was performed on each cell at 750 °C. The results of OCVs and power densities are presented in Figs. 6 and 7. The OCVs and performances of both cells were increased by 5–10% in the first 5 h of test. It can be probably attributed to the conditioning of the electrodes and electrode–electrolyte interfaces. After 5 h, OCV and performance of both cells were gradually dropped. OCVs were slightly decreased with increasing the number of thermal cycles and time (<50 mV after 55 h and 6 thermal cycles of cell test). In contrast, the power densities of both cells were significantly reduced by 25–30 mW cm^{-2} after stability test. Therefore, the performance degradation by operating time and redox cycles in the cell with buffer layer was similar to that for non-buffered cell. A fraction of the power output reduction could be due to the interfacial reactions during operating time. However, the amounts of secondary phases at the different interfaces after operating for 55 h, which were determined by EDX analysis, were the same or slightly higher than those after sintering processes of the different components. It could be due to the relative low temperature and time of the operating test (750 °C) in comparison to the high sintering temperatures, which produced significant interfacial reactions. So, the main contribution for the performance degradation in both cells could be attributed to the degradation of electrodes (reduction of electrode specific area and porosity of some cathode decomposition…) and the interfacial adhesion between the cell components. This fact justified that degradation rates in both cells were similar. In a future work, cell stability should be further enhanced with more measurements at long-time.

4. Conclusions

Performance and short-term stability of electrolyte-supported single-chamber SOFCs were studied using LSGM as an electrolyte and methane as a fuel at intermediate temperatures. The interfacial reaction between the LSGM electrolyte and the anode based on Ni induced a substantial degradation of the cell performance during the sintering process at 1100 °C. It was due to the formation of resistive reaction products, such as $LaSrGa_3O_7$, $LaSrGaO_4$ and $LaNiO_3$, at the anode–electrolyte interface. A SDC buffer layer with a thickness of 10 μm suppressed the anode–electrolyte interfacial

reactions, thus avoiding the La and Ni migration between both cell components. However, the high co-sintering temperature of electrolyte-buffer layer (1400 °C) induced the La diffusion between LSGM and SDC layer, thus obtaining resistive secondary phases ($LaSrGa_3O_7$ and $LaSrGaO_4$) at the buffer–electrolyte interface. As a result, maximum power densities of 246 and 132 mW cm^{-2} were obtained for the buffered and non-buffered cells at 800 °C under optimizing SC-SOFC conditions. The cell performance was not affected operating under optimized conditions: cell temperatures between 680 and 750 °C, and CH_4/O_2 ratios of 1.2–1.7. An electrochemical utilization factor of 1.3% and a cell efficiency of 0.8% were obtained for the cell with buffer layer.

On the other hand, short-term stability tests of cells indicated that the performance degradation, after 55 h of operating time and 6 redox cycles, for the cell with buffer layer was similar to that of non-buffered cell (losing around 25–30 mW cm^{-2}). It could be attributed to that the power output was not strongly affected by the interfacial reactions at operating temperatures equal or below 750 °C. Therefore, the main contribution to the performance degradation in both cells was probably the degradation of electrodes and the interfacial adhesion between the cell components.

Acknowledgements

The present work was financed by the Spanish MICINN under the Projects MAT2008-06785-C02-01-02, MAT2011-23623, and XaRMAE (Xarxa de Referència en Materials Avançats per an l'Energia, Generalitat de Catalunya).

References

[1] M. Yano, A. Tomita, M. Sano, T. Hibino, Solid State Ionics 177 (2007) 3351–3359.
[2] T. Hibino, A. Hashimoto, T. Inoue, J. Tokuno, S. Yoshida, M. Sano, Science 288 (2000) 2031–2033.
[3] Z.P. Shao, C. Kwak, S.M. Haile, Solid State Ionics 175 (2004) 39–46.
[4] T.W. Napporn, X. Jacques-Bedard, F. Morin, M. Meunier, J. Electrochem. Soc. 151 (2004) A2088.
[5] Z.P. Shao, J. Mederos, W.C. Chueh, S.M. Haile, J. Power Sources 162 (2006) 589–596.
[6] T. Hibino, A. Hashimoto, T. Inoue, J. Tokuno, S. Yoshida, M. Sano, J. Electrochem. Soc. 148 (2001) A544–A549.
[7] B.C.H. Steele, J. Power Sources 49 (1994) 1–14.
[8] C. Milliken, S. Guruswamy, A. Khandkar, J. Electrochem. Soc. 146 (1999) 872–878.
[9] H. Inaba, H. Tagawa, Solid State Ionics 83 (1996) 1–16.
[10] M. Feng, J.B. Goodenough, Eur. J. Solid State Inorg. Chem. 31 (1994) 663–672.
[11] T. Ishihara, H. Matsuda, T. Takita, J. Am. Chem. Soc. 116 (1994) 3801–3803.
[12] K. Huang, R. Tichy, J.B. Goodenough, C. Milliken, J. Am. Ceram. Soc. 81 (1998) 2581–2585.
[13] A. Moure, A. Castro, J. Tartaj, C. Moure, J. Power Sources 188 (2009) 489–497.
[14] D. Lee, J.H. Han, E.G. Kim, R.H. Song, D.R. Shin, J. Power Sources 185 (2008) 207–211.
[15] J.H. Wan, J.Q. Yan, J.B. Goodenough, J. Electrochem. Soc. 152 (2005) A1511–A1515.
[16] X. Zhang, S. Ohara, R. Maric, H. Okawa, T. Fukui, H. Yoshida, T. Inagaki, K. Miura, Solid State Ionics 133 (2000) 153–160.
[17] K.N. Kim, B.K. Kim, J.W. Son, J. Kim, H.W. Lee, J.H. Lee, J. Moon, Solid State Ionics 177 (2006) 2155–2158.
[18] M. Rozumek, P. Majewski, H. Schluckwerder, F. Aldinger, J. Am. Ceram. Soc. 87 (2004) 1795–1798.
[19] N. Maffei, G. de Silveria, Solid State Ionics 159 (2003) 209–216.
[20] K. Huang, J.H. Wan, J.B. Goodenough, J. Electrochem. Soc. 148 (2001) A788–A794.
[21] M. Morales, J.J. Roa, X.G. Capdevila, M. Segarra, S. Piñol, Fuel Cells 11 (2011) 108–115.
[22] S.M. Beresnev, B.L. Kuzin, D.I. Bronin, Russ. J. Electrochem 43 (2007) 883.
[23] J.H. Lee, K.N. Kim, J.W.S.J. Kim, B.K. Kim, H.W. Lee, J. Moon, J. Mater. Sci. 42 (2007) 1866.
[24] T. Inagaki, K. Miura, H. Yoshida, R. Maric, S. Ohara, X. Zhang, K. Mukai, T. Fukui, J. Power Sources 86 (2000) 347–351.
[25] C. Bo, C. Yuan, X. Zhao, C.B. Wu, M.Q. Li, Clean Technol. Environ. Policy 11 (2009) 391–399.
[26] H. Zhu, R.J. Kee, J. Power Sources 161 (2006) 957–964.
[27] T. Horita, K. Yamaji, N. Sakai, H. Yokokawa, A. Weber, E. Ivers-Tiffée, Solid State Ionics 138 (2000) 143–152.
[28] A. Naoumidis, A. Ahmad-Khanlou, Z. Samardzija, D. Kolar, J. Anal. Chem. 365 (1999) 277–281.
[29] D. Xu, X. Liu, D. Wang, G. Yi, Y. Gao, D. Zhang, W. Su, J. Alloys Compd. 429 (2007) 292–295.
[30] M. Morales, S. Piñol, M. Segarra, J. Power Sources 194 (2009) 961–966.
[31] T. Fukui, S. Ohara, K. Murata, H. Yoshida, K. Miura, T. Inagaki, J. Power Sources 106 (2002) 142–145.
[32] Z. Shao, S.M. Haile, J. Ahn, P.D. Ronney, Z. Zhan, S.A. Barnett, Nature 435 (2005) 795–798.